

PROFUSE: Efficient Cross-View Context Fusion for Open-Vocabulary 3D Gaussian Splatting

Yen-Jen Chiou Wei-Tse Cheng Yuan-Fu Yang
National Yang Ming Chiao Tung University

remi.ii13@nycu.edu.tw, andy5552555.ii13@nycu.edu.tw, yfyangd@nycu.edu.tw

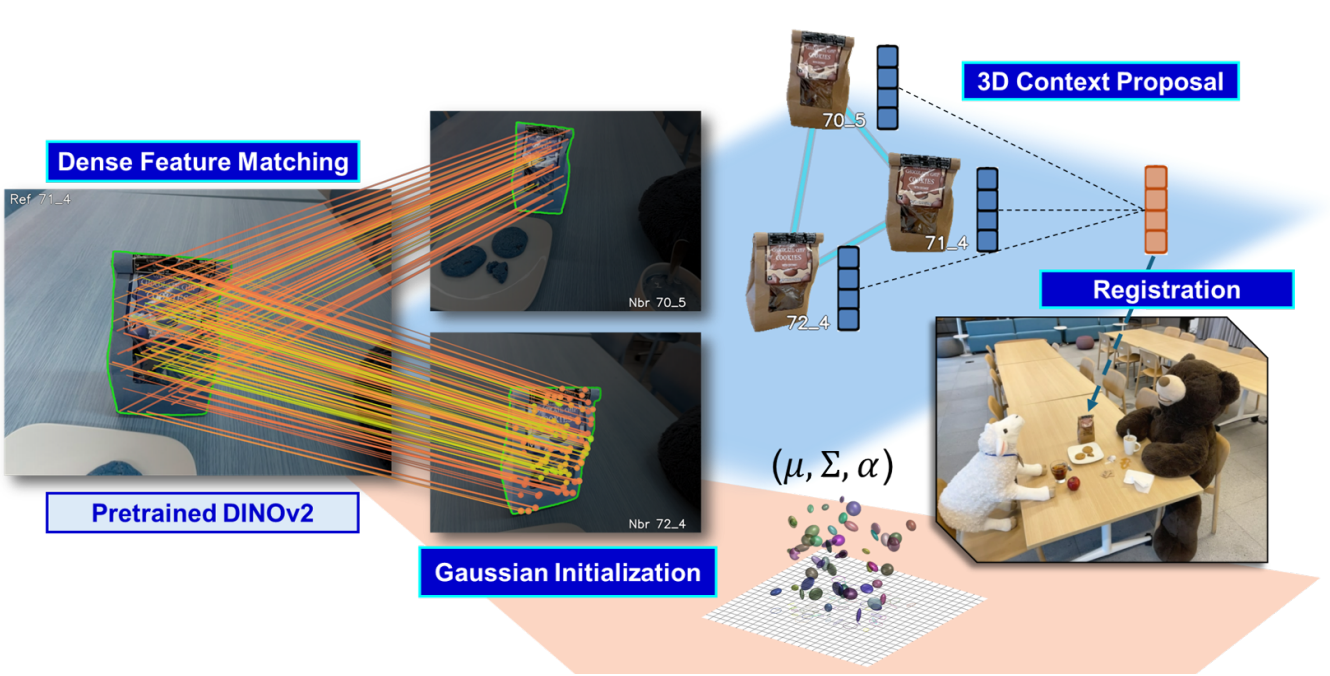


Figure 1. Overview of **ProFuse**. **Left:** A dense matcher supplies cross-view geometric and semantic correspondences. **Top:** Warped masks are grouped into 3D Context Proposals with a shared global feature. **Bottom:** Triangulated matches initialize a compact Gaussian scene, and proposal features are fused without render supervision for coherent open-vocabulary 3D semantics.

Abstract

We present *ProFuse*, an efficient context-aware framework for open-vocabulary 3D scene understanding with 3D Gaussian Splatting (3DGS). The pipeline enhances cross-view consistency and intra-mask cohesion within a direct registration setup, adding minimal overhead and requiring no render-supervised fine-tuning. Instead of relying on a pretrained 3DGS scene, we introduce a dense correspondence-guided pre-registration phase that initializes Gaussians with accurate geometry while jointly constructing 3D Context Proposals via cross-view clustering. Each proposal carries a global feature obtained through weighted aggregation of member embeddings, and this feature is fused

onto Gaussians during direct registration to maintain primitive language coherence across views. With associations established in advance, semantic fusion requires no additional optimization beyond standard reconstruction, and the model retains geometric refinement without densification. *ProFuse* achieves strong open-vocabulary 3DGS understanding while completing semantic attachment in about five minutes per scene, which is 2 \times faster than SOTA. Additional details are available at our project page <https://chiou1203.github.io/ProFuse/>.

1. Introduction

Open-vocabulary 3D scene understanding aims to understand a physical scene using free-form natural language queries, with applications ranging from robotics and autonomous navigation to augmented reality [5, 11, 30, 40, 41, 43]. The task remains challenging, as the system must recover accurate geometry while also assigning meaningful semantic concepts without being restricted to fixed labels. Earlier efforts explored a range of 3D representations [10, 12, 15, 23, 25, 33, 40]. Recent work has focused on 3D Gaussian Splatting [14], which represents a scene as a set of anisotropic Gaussians and enables photo-realistic, real-time rendering.

Early work adopts 2D vision–language distillation in which images are rendered during training and Gaussian features are optimized to match 2D predictions [9, 27, 34, 42, 44]. This pipeline can propagate open-vocabulary knowledge into 3D, but it also introduces two structural issues. The supervision signal is delivered only after rendering and compositing, leading to mismatches with the original language embedding that described the region. In addition, semantics are acquired and queried through individual views, making reasoning less direct and less stable. These limitations have motivated methods that operate directly in 3D Gaussian space [13, 20, 28, 39]. These approaches assign language features to each Gaussian and answer a text query by comparing the query embedding with those per-Gaussian features in 3D.

More recent work has moved toward a registration-based formulation [13]. This approach bypasses render-supervised semantic training. Language-aligned features are directly registered in Gaussians using their visibility along each viewing ray. The result is a compact, queryable 3D semantic field with high efficiency. Despite such progress, the direct registration paradigm is still in its early stages. Our aim is to strengthen the registration framework by injecting semantic consistency into the 3DGS representation without any additional render-supervised training.

We propose a registration-based framework ProFuse that strengthens semantic coherence in 3D Gaussian Splatting. Our key insight is to enforce two key factors highlighted by previous work [32, 35, 39, 42], namely cross-view consistency and intra-mask cohesion. Prior approaches typically encourage these properties through render-supervised training on 2D feature maps or through explicit feature-learning objectives. The registration pipeline does not impose these constraints. Our approach injects these forms of semantic consistency directly into the registration framework.

An overview of the proposed pipeline is shown in Figure 1. We introduce a pre-registration stage guided by dense multi-view correspondence [8]. The correspondence signal initializes the 3D Gaussian scene with accurate geometry [17], which allows the representation to cover the scene

without relying on iterative densification. The same signal is also used to connect observations of the same object across different viewpoints, consolidating them into consistent, object-level groups that we refer to as 3D Context Proposals. Each 3D Context Proposal encodes an object as it appears across views, rather than as an isolated per-frame mask, and provides a stable source of semantics that is aligned across viewpoints.

During feature registration, each proposal carries a global language feature computed from its mask members. We then assign each Gaussian to its corresponding context proposals and associate the global semantics to the Gaussian. Notably, our method does not involve gradient-based fine-tuning or backpropagation of language loss. Through experiments across open-vocabulary 3D perception tasks, we demonstrate effectiveness in 3D object selection, open-vocabulary point cloud understanding, and optimizing efficiency. Our contributions are summarized as follows:

- A registration-based semantic augmentation of 3D Gaussian Splatting that introduces cross-view semantic consistency and intra-mask coherence without any render-supervised training for semantics.
- A pre-registration stage driven by dense multi-view correspondence. The same correspondence signal initializes a well-covered 3D Gaussian scene and assembles consistent mask evidence across views into 3D Context Proposals.
- A unified open-vocabulary 3D scene representation that improves object selection, point cloud understanding, and training efficiency on existing benchmarks while maintaining render-free semantic association efficiently.

Overall, ProFuse offers a compact and training-free route to consistent open-vocabulary 3D scene understanding built directly on correspondence-driven registration.

2. Related Work

Neural rendering has progressed from NeRFs to explicit point-based primitives [1, 21, 22]. 3DGS provides fast, spatially local rendering and is now a common backbone for open-vocabulary understanding [14, 36]. Render-supervised distillation methods transfer 2D vision–language signals into 3D by supervising rendered feature maps [9, 12, 15, 25, 27, 29, 34, 35, 37, 44]. Direct 3D retrieval attaches language-aligned descriptors to Gaussians or points for volumetric querying [13, 20, 28, 39]. To stabilize semantics across views, recent works encourage cross-view consistency and semantic cohesion [3, 4, 12, 18, 20, 25, 26, 35, 37, 39, 42]. Finally, dense correspondence provides wide-baseline matches and confidences useful for multi-view grouping and correspondence-driven 3DGS initialization [2, 7, 8, 17, 19, 31, 38]. We build on this direction to couple correspondence-guided context association with registration-based semantic field.

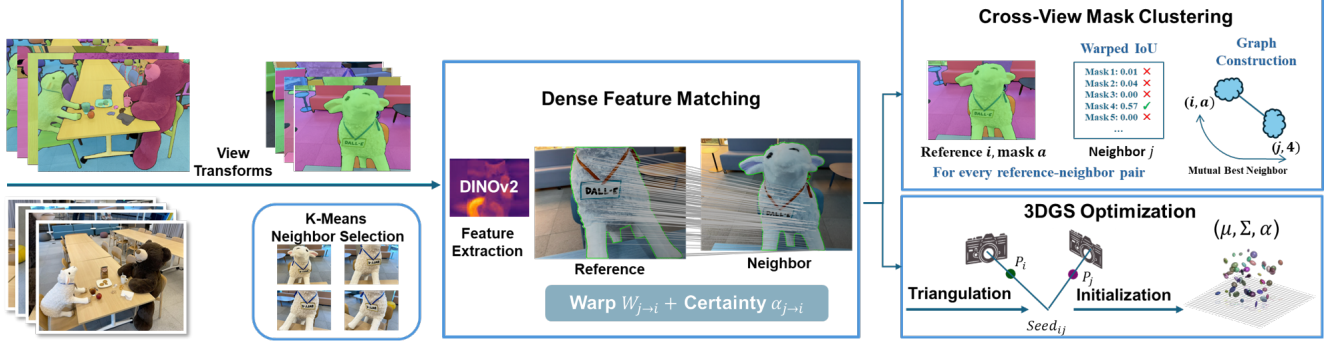


Figure 2. **Pre-registration.** For each reference view we select K neighbors via view clustering, then apply a pre-trained dense matcher to obtain per-pixel warps $W_{j \rightarrow i}$ and confidences $\alpha_{j \rightarrow i}$. **Bottom right:** Given the warps of a *pixel pair*, we triangulate a 3D seed point for Gaussian initialization. **Top right:** Warped IoU comparison on every reference–neighbor *mask pair*; masks that pass the selection form edges of a bipartite graph.

3. Method

We construct a semantic 3D Gaussian scene that can be queried with natural language without any render-supervised semantic training. The pipeline begins with a pre-registration stage via dense correspondence. This stage initializes a dense Gaussian scene and links segmentation masks across views to form 3D Context Proposals. Each proposal records which masks across views are inferred to refer to the same scene content, giving us cross-view groupings before any semantic fusion. A context-guided registration stage then uses these proposals to compute a global language feature for each proposal. The features are then assigned to the corresponding Gaussians using visibility-based weights derived from transmittance and opacity along camera rays. The final output is a 3D representation with cross-view consistency and intra-mask cohesion that can be searched directly in 3D by a text query.

3.1. Dense Correspondence Pre-registration

The pre-registration process begins from a set of posed RGB images of a scene. Let $\{I_i\}_{i=1}^N$ denote input views, and let each image I_i have known camera intrinsics and extrinsics. The goal of this stage is to initialize a dense set of 3D Gaussians with accurate geometry and initial appearance attributes, and to record cross-view evidence for semantic grouping. As an overview, the full pre-registration workflow is visualized in Figure 2.

For each image I_i , we obtain a set of non-overlapping region masks $\{M_i^k\}$ using SAM [16], where $M_i^k \in \{0, 1\}^{H \times W}$ is a binary mask for the region k in view i . For every mask M_i^k , we extract a language-aligned feature vector $f_i^k \in \mathbb{R}^D$ by cropping the corresponding region in I_i and encoding it with CLIP [29]. The result is a per-view dictionary $\mathcal{S}_i = \{(M_i^k, f_i^k) \mid k = 1, \dots, K_i\}$, where K_i is the number of predicted regions in view i . The sets \mathcal{S}_i will later serve as semantic evidence.

Dense Feature Matching. To relate content across views, we compute dense correspondences between pairs of images using a pretrained dense matching network (see Figure 2). The network was trained on a coarse layer using DINOv2 [24] and a fine layer with pyramid convolution. The result is a robust dense feature matching.

Given two images I_i and I_j , the dense matcher returns $C(I_i, I_j) \rightarrow W_{j \rightarrow i}, \alpha_{j \rightarrow i}$, where $W_{j \rightarrow i} \in \mathbb{R}^{2 \times H \times W}$ is a dense warp field that maps each pixel coordinate (u, v) in I_j to a subpixel coordinate in I_i , and $\alpha_{j \rightarrow i} \in \mathbb{R}^{H \times W}$ is a confidence map. Intuitively, $W_{j \rightarrow i}(u, v)$ predicts where the content seen at (u, v) in view j should appear in view i . The value $\alpha_{j \rightarrow i}(u, v)$ measures how reliable that match is. We discard correspondences whose confidence falls below a threshold. The result is a dense set of pixel-to-pixel matches across views that remains stable under wide viewpoint change.

Gaussian Initialization. We use the high-confidence correspondences to seed 3D Gaussian primitives directly in space. For a confident match between the pixel (u_j, v_j) in view j and its mapped location (u_i, v_i) in view i , we back-project both pixels into 3D using known camera poses and triangulate their intersection. The resulting 3D point becomes the initial center of a Gaussian (see Figure 2, bottom right). Its initial appearance attributes are taken from the supporting image evidence, and its initial scale and orientation are set to cover a small spatial neighborhood around that 3D point. Repeating this over correspondences yields the initial Gaussian set $\mathcal{G}_0 = \{g_n\}$, where each g_n is a Gaussian primitive with position, scale, orientation, opacity, and color. Because these Gaussians are instantiated from dense correspondences rather than grown through iterative densification, \mathcal{G}_0 already provides broad and near-uniform spatial coverage of the scene. Subsequent geometric refinement adjusts these primitives but does not need to create a large number of new Gaussians.

Algorithm 1 Cross-view mask clustering

```

1: Inputs: per-view sets  $\{\mathcal{S}_i\}$  with  $\mathcal{S}_i = \{(M_i^k, f_i^k)\}$ ;  

   dense warp field  $W_{j \rightarrow i}$  and certainties  $\alpha_{j \rightarrow i}$ ; visibility  

   mask; thresholds  $\tau_\alpha$ ,  $\tau_{iou}$ ,  $\tau_{box}$ ; size gates  $s_{min}$ ,  $v_{min}$ .  

2: Initialize graph  $G = (V, E)$  with  $V \leftarrow \{(i, k) \forall M_i^k\}$ ,  

    $E \leftarrow \emptyset$   

3: for all ordered view pairs  $(i, j)$  do  

4:    $\Gamma_{j \rightarrow i} \leftarrow [\alpha_{j \rightarrow i} \geq \tau_\alpha] \wedge \text{vis\_mask}$   

5:   for all mask pairs  $(M_i^a, M_j^b)$  do  

6:      $\tilde{M}_{j \rightarrow i}^b \leftarrow \mathcal{W}(M_j^b; W_{j \rightarrow i})$   

7:      $O_{i,a;j,b} \leftarrow \text{IoU}(M_i^a \odot \Gamma_{j \rightarrow i}, \tilde{M}_{j \rightarrow i}^b \odot \Gamma_{j \rightarrow i})$   

8:      $\tilde{M}_{i \rightarrow j}^a \leftarrow \mathcal{W}(M_i^a; W_{i \rightarrow j})$   

9:      $O_{j,b;i,a} \leftarrow \text{IoU}(M_j^b \odot \Gamma_{i \rightarrow j}, \tilde{M}_{i \rightarrow j}^a \odot \Gamma_{i \rightarrow j})$   

10:     $B_{i,a;j,b} \leftarrow \text{BBoxIoU}(M_i^a, \tilde{M}_{j \rightarrow i}^b)$   

11:     $B_{j,b;i,a} \leftarrow \text{BBoxIoU}(M_j^b, \tilde{M}_{i \rightarrow j}^a)$   

12:    if  $O_{i,a;j,b} \geq \tau_{iou}$  and  $O_{j,b;i,a} \geq \tau_{iou}$  and  

         $B_{i,a;j,b} \geq \tau_{box}$  and  $B_{j,b;i,a} \geq \tau_{box}$  then  

13:      Add undirected edge between  $(i, a)$  and  

         $(j, b)$  to  $E$   

14:    end if  

15:  end for  

16: end for  

17: Extract connected components  $\{\mathcal{C}_m\}$  of  $G$   

18: Filter  $\mathcal{C}_m$  by  $|\mathcal{C}_m| \geq s_{min}$  and  $|\text{views}(\mathcal{C}_m)| \geq v_{min}$   

19:  $\mathcal{P} \leftarrow \{P_m \equiv \mathcal{C}_m\}$   

20: return  $\mathcal{P}$ 


---



```

Cross-view Context Association. The same correspondence field lets us record which masks from different views refer to the same scene content. Consider two masks M_i^a from view i and M_j^b from view j . We project M_j^b into view i using the warp field $W_{j \rightarrow i}$, producing a warped support mask in the coordinates of I_i . We then measure how well this warped support overlaps M_i^a , restricted to pixels with high correspondence confidence $\alpha_{j \rightarrow i}$. If the overlap exceeds a threshold, we register a link that these two masks are consistent observations of the same underlying scene content. Repeating this procedure over view pairs accumulates the link set $\mathcal{L} = \{(M_i^a, \tilde{M}_{j \rightarrow i}^b)\}$, where each pair in \mathcal{L} indicates strong cross-view agreement between two masks (see Figure 2, top right).

The pre-registration stage produces two artifacts. The first is an initialized Gaussian scene \mathcal{G}_0 created by triangulating dense correspondences. The second is a pool of mask links across views \mathcal{L} that captures which regions per-view act as the same scene content between viewpoints. Section 3.2 addresses how we cluster masks in \mathcal{L} into 3D Context Proposals.

3.2. 3D Context Proposals

3D Context Proposals are formed through grouping per-view masks that mutually support one another under dense correspondence into stable multi-view units. We realize this by testing pairwise agreements under correspondence warps and linking masks that pass mutual gates; connected components in the resulting graph define the proposals.

Cross-view Mask Clustering. Algorithm 1 demonstrates the clustering procedure. Let a mask node be $m = (i, k)$ with $M_i^k \in \{0, 1\}^{H \times W}$. Given a candidate pair (i, a) and (j, b) with a dense warp $W_{j \rightarrow i}$ from view j to i and a certainty map $\alpha_{j \rightarrow i}$, we gate matches using a fixed certainty threshold $\tau_\alpha \in [0, 1]$ together with a renderer-derived visibility mask `vis_mask`. The binary gate is defined as

$$\Gamma_{j \rightarrow i} = [\alpha_{j \rightarrow i} \geq \tau_\alpha] \wedge \text{vis_mask}. \quad (1)$$

The warped support in view i is obtained as

$$\tilde{M}_{j \rightarrow i}^b = \mathcal{W}(M_j^b; W_{j \rightarrow i}), \quad (2)$$

where \mathcal{W} denotes bilinear sampling at sub-pixel accuracy. The confidence-gated overlap in view i is

$$O_{i,a;j,b} = \text{IoU}\left(M_i^a \odot \Gamma_{j \rightarrow i}, \tilde{M}_{j \rightarrow i}^b \odot \Gamma_{j \rightarrow i}\right). \quad (3)$$

We compute a coarse bounding-box agreement $B_{i,a;j,b} = \text{IoU}(\text{box}(M_i^a), \text{box}(\tilde{M}_{j \rightarrow i}^b))$ and gate links with two thresholds, τ_{iou} for mask overlap and τ_{box} for box overlap. Agreement is required in both directions, and an undirected link is accepted only if

$$\begin{aligned} O_{i,a;j,b} &\geq \tau_{iou} \quad \text{and} \quad O_{j,b;i,a} \geq \tau_{iou}, \\ B_{i,a;j,b} &\geq \tau_{box} \quad \text{and} \quad B_{j,b;i,a} \geq \tau_{box}. \end{aligned} \quad (4)$$

A graph $G = (V, E)$ is then constructed with vertices $V = \{(i, k)\}$. For every cross-view pair that passes the mutual gates above, we add an undirected edge to E . The connected components of G define the raw proposals. Very small components are removed using two criteria: minimal member count s_{min} and minimal distinct-view support v_{min} . Each proposal P_m is represented only by its membership list (i, k) , contributing view set, and compact per-view label maps for efficient lookup.

3.3. Feature Registration

The goal of the registration stage is to assign a unit-normalized language descriptor to every Gaussian, enabling text queries to be evaluated directly in 3D. This stage operates on the initialized Gaussian set \mathcal{G}_0 , calibrated cameras, the per-view mask dictionary $\mathcal{S}_i = \{(M_i^k, f_i^k)\}$, and the proposal set $\mathcal{P} = \{P_m\}$ constructed in §3.2.

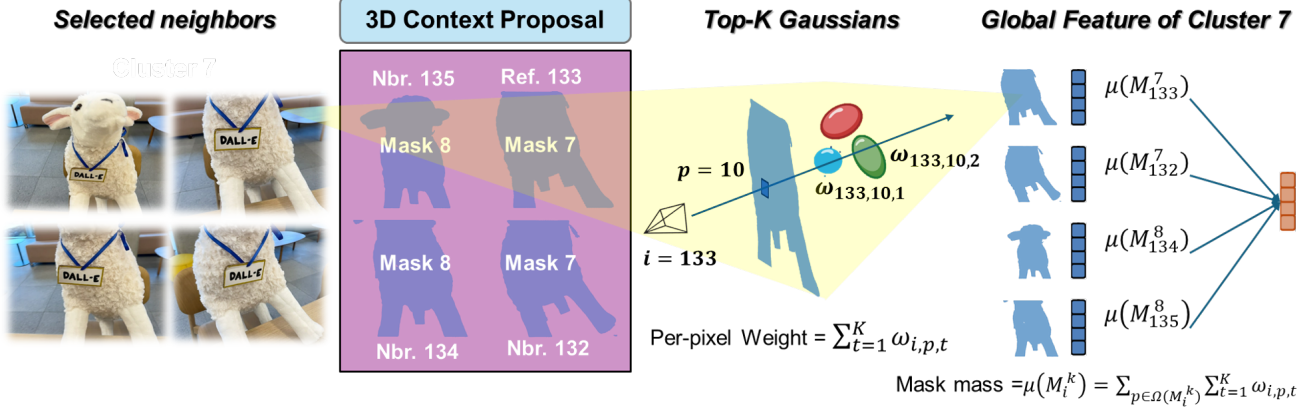


Figure 3. **From context proposal to global feature.** Left: masks of the same entity are grouped into a 3D Context Proposal. Center: for a pixel p , the renderer returns the top- K Gaussians with contributions $\{\omega_{i,p,t}\}_{t=1}^K$, from which the *mask mass* $\mu(M_i^k)$ is computed. Right: a mass-weighted pool of member mask embeddings forms the proposal feature, which is registered to Gaussians via Eq. (8).

For a view i and a pixel p , the renderer returns the indices and weights of the top- K Gaussians along the ray, denoted $\{(g_{i,p,t}, \omega_{i,p,t})\}_{t=1}^K$. Their blending contributions are

$$\begin{aligned} \omega_{i,p,t} &= T_{i,p,t} \alpha_{i,p,t}, \\ T_{i,p,t} &= \prod_{s < t} (1 - \alpha_{i,p,s}), \end{aligned} \quad (5)$$

where $\alpha_{i,p,t}$ is the effective opacity and $T_{i,p,t}$ is the transmittance of the preceding Gaussians on the ray.

Each proposal P_m contains member masks drawn from multiple views. We compute a scalar *mass* for every mask by integrating renderer contributions over the mask pixels

$$\mu(M_i^k) = \sum_{p \in \Omega(M_i^k)} \sum_{t=1}^K \omega_{i,p,t}. \quad (6)$$

The proposal descriptor is a mass-weighted pool of mask embeddings followed by ℓ_2 normalization,

$$\bar{f}_m = \frac{\sum_{(i,k) \in P_m} \mu(M_i^k) f_i^k}{\left\| \sum_{(i,k) \in P_m} \mu(M_i^k) f_i^k \right\|_2}. \quad (7)$$

An illustration of this aggregation is provided in Figure 3.

A pixel-wise proposal map $L_i(p)$ is constructed for every training view, assigning each pixel inside a mask to the ID of its corresponding proposal in \mathcal{P} . Pixels outside all masks receive a null label and are ignored. For each Gaussian $g \in \mathcal{G}_0$, a feature accumulator $A[g] \in \mathbb{R}^D$ and a scalar weight sum $S[g] \in \mathbb{R}_{\geq 0}$ are initialized to zero. For every pixel p with valid proposal $m = L_i(p)$ and each of its top- K hits, the accumulation step is

$$\begin{aligned} A[g_{i,p,t}] &\leftarrow A[g_{i,p,t}] + \omega_{i,p,t} \bar{f}_m, \\ S[g_{i,p,t}] &\leftarrow S[g_{i,p,t}] + \omega_{i,p,t}. \end{aligned} \quad (8)$$

This registration step consumes the proposal feature from Figure 3 and weights it by contributions $\omega_{i,p,t}$.

After processing all views, the descriptor for Gaussian g is computed as

$$f_g = \frac{A[g]}{\max(S[g], \varepsilon)}, \quad \hat{f}_g = \frac{f_g}{\|f_g\|_2}, \quad (9)$$

with a small ε for numerical stability. The implementation uses batched gather-scatter operations and relies only on renderer outputs.

3.4. Inference Procedure

A text query is encoded to $f_q \in \mathbb{R}^D$ and normalized as $\hat{f}_q = f_q / \|f_q\|_2$. Each Gaussian g stores a registered descriptor from §3.3. Following Dr. Splat [13], Product Quantization (PQ) is used for memory-efficient retrieval. Descriptors are stored as FAISS product-quantized codes and decoded to unit-normalized vectors at query time.

Cosine similarity is used to score Gaussians, $s_g = \hat{f}_q^\top \hat{f}_g$. A FAISS PQ index over $\{\hat{f}_g\}$ produces a shortlist that is re-scored using decoded (full-precision) descriptors. Selection is performed directly in 3D without any render-based fine-tuning: a Gaussian is considered active if $s_g \geq \tau_{\text{act}}$. For visualization in view i , let $\{(g_{i,p,t}, \omega_{i,p,t})\}_{t=1}^K$ denote the Top- K contributors to pixel p . The activation mask is defined as

$$M_i(p) = \mathbb{1}[A_i(p) \geq \gamma], \quad (10)$$

where $A_i(p)$ is the sum of contributions over Top- K hits.

4. Experiments

4.1. Implementation

Experiments are conducted on the LERF-OVS [15] and ScanNet [6] datasets. All four LERF scenes are used, and 10 scenes are sampled from the ScanNet dataset. SAM-based segmentation and mask embedding are preprocessed on 8 NVIDIA H100 GPUs, while all remaining experiments run on a single A100 GPU.

Table 1. Evaluation of 3D object selection on LERF-OVS [15] dataset. Scores are averaged per scene and then across scenes. Bold indicates the best performance.

Method	mIoU \uparrow					mAcc@0.25 \uparrow				
	waldo kitchen	figurines	ramen	teatime	mean	waldo kitchen	figurines	ramen	teatime	mean
LangSplat	9.18	10.16	7.92	11.38	9.66	9.09	11.27	8.93	20.34	12.41
LEGaussians	11.78	17.99	15.79	19.27	16.21	18.18	23.21	26.76	27.12	23.82
OpenGaussian	24.57	53.01	24.44	55.40	39.36	36.36	83.93	39.44	76.27	59.00
Dr. Splat	29.37	51.73	26.32	55.53	40.74	50.00	82.14	40.85	79.66	63.16
ProFuse (Ours)	36.91	56.13	28.16	62.78	46.00	68.18	85.71	39.44	79.66	68.25

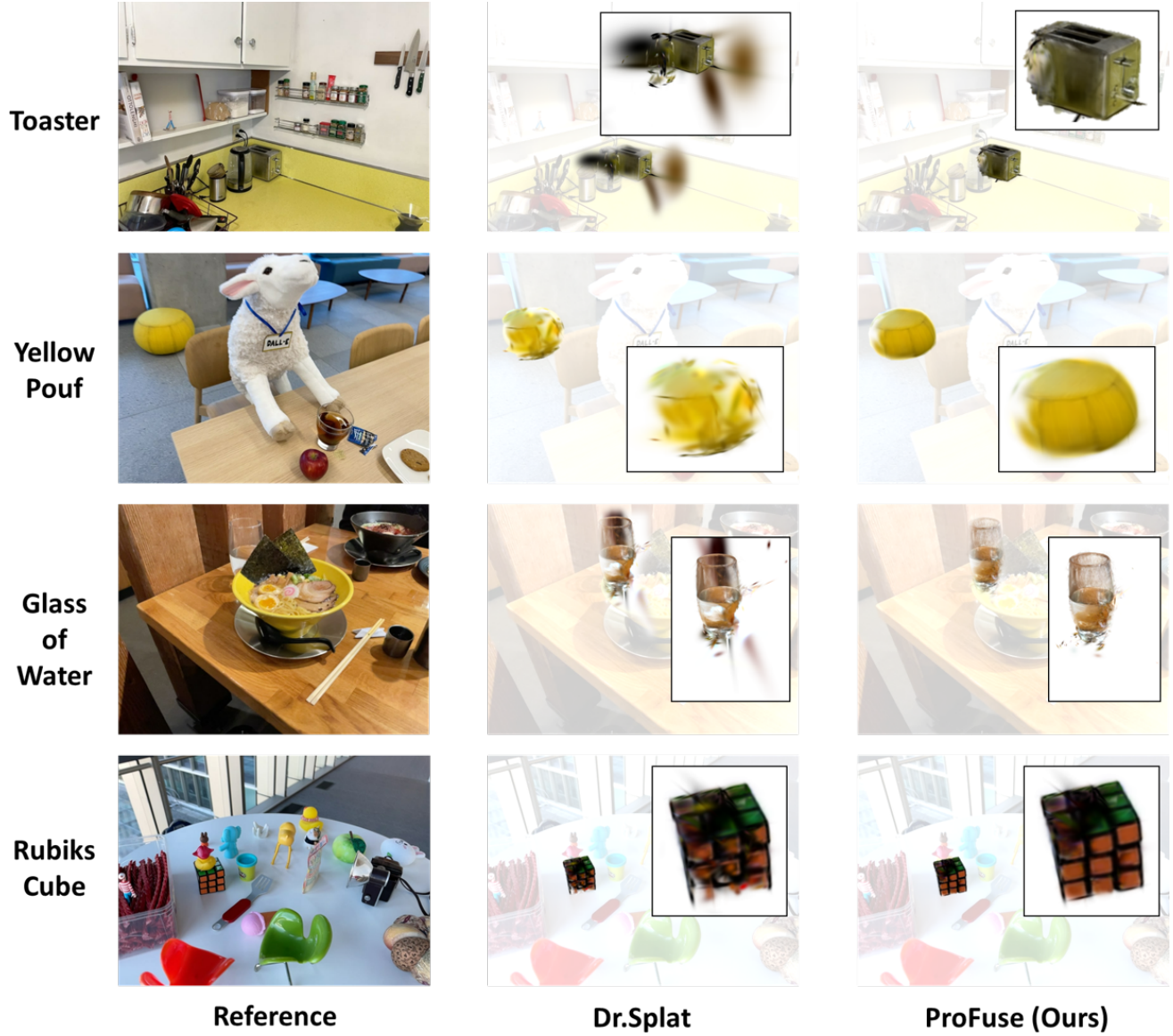


Figure 4. Qualitative comparison of object-level semantic queries on the LERF-OVS [15] dataset. Our method produces more accurate and cleaner object retrieval, showing sharper correspondence between the text query and the selected 3D content.

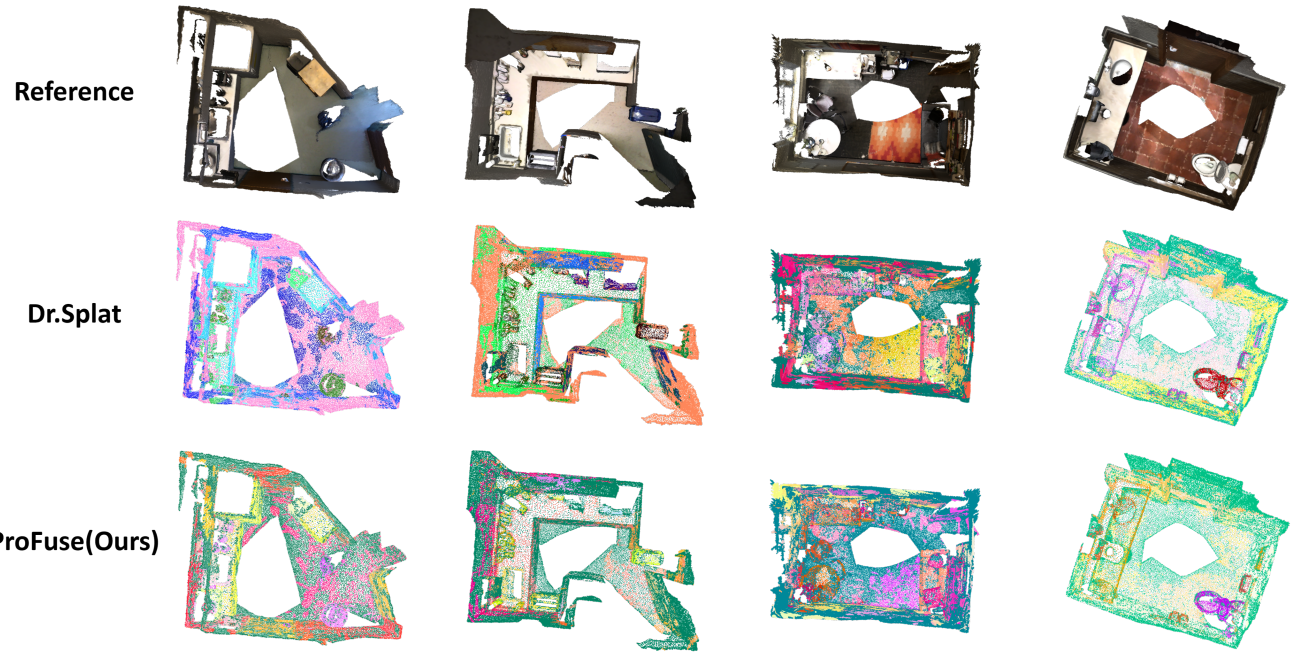


Figure 5. Feature visualizations on the ScanNet [6] dataset using registration-based methods. Colors represent normalized language features transferred to mesh vertices and rendered via a fixed RGB projection. ProFuse produces cleaner regions with sharper boundaries and fewer speckles.

4.2. Open-Vocabulary 3D Object Selection

We evaluate open-vocabulary 3D object selection on the four LERF scenes using the official text queries and splits. Each method outputs a binary activation per frame, while our pipeline performs selection directly in 3D. Let $q \in \mathbb{R}^D$ be the CLIP text embedding, normalized as $\hat{q} = q / \|q\|_2$. Each Gaussian g stores a normalized language feature \hat{f}_g from registration. Active Gaussians are defined as $\mathcal{G}_\tau = \{g \mid \langle \hat{f}_g, \hat{q} \rangle \geq \tau\}$, with a method-specific global threshold τ . For view i and pixel p , the renderer provides the top- K Gaussians and weights $\omega_{i,p,t}$. The activation is

$$A_i(p) = \sum_{t=1}^K \omega_{i,p,t} \mathbf{1}[g_{i,p,t} \in \mathcal{G}_\tau],$$

and the mask is $\widehat{M}_i = \mathbf{1}[A_i \geq \gamma]$ using a fixed silhouette threshold γ . A small grid search is used to determine the global threshold τ for each method. *mean IoU* is computed by evaluating intersection-over-union for each query-frame pair and averaging across all queries and frames in a scene. The final score is obtained by averaging across the four scenes. Table 1 reports these quantitative results. The metric *mAcc@0.25* is also provided, defined as the fraction of query-frame pairs with IoU at least 0.25, using the same τ .

Table 2. Open-vocabulary point cloud understanding on ScanNet. Results use mIoU and mAcc for 19/15/10-class settings.

Method	19 classes		15 classes		10 classes	
	mIoU↑	mAcc↑	mIoU↑	mAcc↑	mIoU↑	mAcc↑
LangSplat	3.78	9.11	5.35	13.20	8.40	22.06
LEGaussians	3.84	10.87	9.01	22.22	12.82	28.62
OpenGaussian	24.73	41.54	30.13	48.25	38.29	55.19
Dr. Splat	28.40	52.77	32.67	58.53	36.81	66.41
ProFuse (Ours)	30.52	55.32	34.76	60.90	39.74	69.38

Qualitative results are presented in Figure 4. Our method isolates the queried object with far fewer background activations, yielding cleaner and more semantically precise selections. In contrast, Dr. Splat often exhibit ray-like spillovers into nearby clutter or textured areas. For instance, the “Toaster” query incorrectly highlights the entire kettle on the left, while the “Glass of Water” query becomes distract by specular reflections.

4.3. Open-Vocabulary Point Cloud Understanding

The evaluation is conducted on the ScanNet dataset using the label spaces defined in OpenGaussian [39], considering class sets of 19, 15, and 10 categories. Each mesh vertex in the aligned reconstruction is assigned a semantic label, and

Table 3. Comparison of training requirements and retrieval speed across 3D scene understanding methods.

Method	Scene	Render supervision	Feature distill.	Query
LERF	NeRF	required	~24 h	slow
LangSplat	SfM-3DGS	required	~4 h	slow
LEGaussians	SfM-3DGS	required	~4 h	slow
OpenGaussian	SfM-3DGS	required	~1 h	fast
GOI	SfM-3DGS	required	~12 min	fast
Dr. Splat	SfM-3DGS	none	~10 min	fast
ProFuse (Ours)	Corr-init 3DGS	none	~5 min	fast

class names are encoded once into language embeddings and reused across all methods.

Per-Gaussian language codes are first decoded using FAISS PQ to obtain cosine logits against class embeddings. These logits are transferred to mesh vertices through a spatially aware kernel that respects each Gaussian’s full ellipsoid. Candidate Gaussians are shortlisted by Euclidean proximity ($K=64$), filtered by an elliptical Mahalanobis gate ($\sigma=3$), and weighted by both $\exp(-\frac{1}{2}d^2)$ and Gaussian opacity. A softmax over class logits yields per-candidate class probabilities, and vertex scores are computed as the weighted sum of all candidates. Because predictions occur directly in 3D, no rendering is involved during evaluation. The same kernel and shortlist configuration is applied to every method so that performance differences reflect the quality of the learned Gaussian features rather than variations in the transfer rule. Ten scenes from ScanNet are sampled for evaluation, and scores are computed with fixed hyper-parameters to report average *mIoU* and *mAcc* for each class set. Quantitative results for the 19-, 15-, and 10-class settings are provided in Table 2.

To contextualize point-level scores, we visualize feature colorings of ScanNet reconstructions and compare them to the pioneer registration-based baseline Dr. Splat [13] in Figure 5. For each scene, we show the reference mesh view and two pseudo-colored point clouds. Colors are obtained by projecting normalized per-Gaussian features to three channels and painting the transferred per-vertex features; views are matched to the reference for consistent framing. Dr. Splat tends to produce darker, patchy fragments and color bleeding near corners, whereas our results exhibit higher region consistency with large surfaces rendered in coherent color swaths. We achieve cleaner boundaries at furniture edges and fixtures with fewer mixed colors at object–wall contacts.

4.4. Training Efficiency

The cost of attaching open-vocabulary semantics to a reconstructed scene is measured in wall-clock time. As shown in Table 3, render-supervised distillation methods require hours of processing, and existing registration-based approaches [13] still take several minutes. ProFuse achieves the fastest runtime through correspondence-guided initial-

Table 4. Wall-clock comparison of geometry, semantic processing, and indexing time on the LERF dataset.

Method	Geometry	Semantics	Total	Indexing
OpenGaussian	~20 m	~40 m	~1 h	Codebook
Dr. Splat	~20 m	~0 + 10 m	~30 m	PQ
ProFuse (Ours)	~2 + 15 m	~2m + 20 s	~19 m	PQ

Table 5. Top- K analysis on ScanNet showing mIoU and feature registration time for registration-based methods.

Method	Top $K=10$		Top $K=20$		Top $K=40$	
	mIoU↑	time↓	mIoU↑	time↓	mIoU↑	time↓
Dr. Splat	33.82	~45 s	35.57	~85 s	36.81	~165 s
ProFuse (Ours)	39.74	~25 s	39.74	~25 s	39.74	~25 s

ization, which produces a compact Gaussian set without densification, and through lightweight proposal-level feature fusion. These components reduce semantic attachment to about five minutes per scene, making ProFuse 2x faster than the prior SOTA. Table 4 provides a runtime breakdown of direct 3D methods. ProFuse reduces scene-specific semantic association to only a few minutes because proposal construction is lightweight and registration uses simple contribution accumulation without gradient updates. The compact geometry from correspondence-guided initialization removes densification and further shortens processing time.

4.5. Ablation Study

To isolate the effect of correspondence-guided geometry and context proposals, we study the impact of the Top-K Gaussian candidates used during feature registration. Table 5 reports mIoU and registration time on ScanNet under three settings $K=10, 20, 40$. Without context proposals, registration-based baselines typically require $K=40$ to achieve saturation, indicating weak concentration of semantic mass along the viewing ray. In contrast, ProFuse reaches its maximum accuracy with $K=10$. The global proposal features place most of the mass on the leading few Gaussians, while our correspondence-initialized geometry further reduces long-tail ambiguity. As a consequence, larger K offers no additional benefit, and a compact $K=10$ is sufficient for both accuracy and speed.

5. Conclusion

ProFuse enforces cross-view semantic consistency in 3DGS without requiring any render-supervised learning for semantics. Dense correspondences generate 3D Context Proposals, and visibility-weighted fusion yields a coherent semantic field. Experiments on LERF and ScanNet confirm accurate open-vocabulary selection and point-level understanding, showing that correspondence-guided geometry provides an efficient path to semantic association in 3DGS.

References

[1] Jonathan T. Barron, Ben Mildenhall, Matthew Tancik, Peter Hedman, Ricardo Martin-Brualla, and Pratul P. Srinivasan. Mip-nerf: A multiscale representation for anti-aliasing neural radiance fields. In *ICCV*, 2021. 2

[2] Naijian Cao, Renjie He, Yuchao Dai, and Mingyi He. Loflat: Local feature matching using focused linear attention transformer. *arXiv preprint arXiv:2410.22710*, 2024. 2

[3] Jiazhong Cen, Jiemin Fang, Chen Yang, Lingxi Xie, Xiaopeng Zhang, Wei Shen, and Qi Tian. Segment any 3d gaussians. In *AAAI*, 2025. 2

[4] Rohan Chacko, Nicolai Haeni, Eldar Khaliullin, Lin Sun, and Douglas Lee. Lifting by gaussians: A simple, fast and flexible method for 3d instance segmentation. *arXiv preprint arXiv:2502.00173*, 2025. 2

[5] Jianchuan Chen, Jingchuan Hu, Gaige Wang, Zhonghua Jiang, Tiansong Zhou, Zhiwen Chen, and Chengfei Lv. Taoavtar: Real-time lifelike full-body talking avatars for augmented reality via 3d gaussian splatting. In *CVPR*, 2025. 2

[6] Angela Dai, Angel X. Chang, Manolis Savva, Maciej Halber, Thomas Funkhouser, and Matthias Nießner. Scannet: Richly-annotated 3d reconstructions of indoor scenes. In *CVPR*, 2017. 5, 7

[7] Johan Edstedt, Ioannis Athanasiadis, Mårten Wadenbäck, and Michael Felsberg. Dkm: Dense kernelized feature matching for geometry estimation. *arXiv preprint arXiv:2202.00667*, 2022. 2

[8] Johan Edstedt, Qiyu Sun, Georg Bökman, Mårten Wadenbäck, and Michael Felsberg. Roma: Robust dense feature matching. *arXiv preprint arXiv:2305.15404*, 2023. 2

[9] Jun Guo, Xiaojian Ma, Yue Fan, Huaping Liu, and Qing Li. Semantic gaussians: Open-vocabulary scene understanding with 3d gaussian splatting. *arXiv preprint arXiv:2403.15624*, 2024. 2

[10] Qingdong He, Jinlong Peng, Zhengkai Jiang, Kai Wu, Xiaozhong Ji, Jiangning Zhang, Yabiao Wang, Chengjie Wang, Mingang Chen, and Yunsheng Wu. Unim-ov3d: Unimodality open-vocabulary 3d scene understanding with fine-grained feature representation. In *IJCAI*, 2024. 2

[11] Chenguang Huang, Oier Mees, Andy Zeng, and Wolfram Burgard. Visual language maps for robot navigation. In *ICRA*, London, UK, 2023. 2

[12] Krishna Murthy Jatavallabhula, Alihusein Kuwajerwala, Qiao Gu, Mohd Obama, Tao Chen, Shuang Li, Ganesh Iyer, Soroush Saryazdi, Nikhil Keetha, Ayush Tewari, Joshua B. Tenenbaum, Celso Miguel de Melo, Madhava Krishna, Liam Paull, Florian Shkurti, and Antonio Torralba. Conceptfusion: Open-set multimodal 3d mapping. *Robotics: Science and Systems (RSS)*, 2023. 2

[13] Kim Jun-Seong, Kim GeonU, Kim Yu-Ji, Yu-Chiang Frank Wang, Jaesung Choe, and Tae-Hyun Oh. Dr. splat: Directly referring 3d gaussian splatting via direct language embedding registration. In *CVPR*, 2025. 2, 5, 8

[14] Bernhard Kerbl, Georgios Kopanas, Thomas Leimkühler, and George Drettakis. 3d gaussian splatting for real-time radiance field rendering. *ACM Transactions on Graphics*, 42(4), 2023. 2

[15] Justin Kerr, Chung Min Kim, Ken Goldberg, Angjoo Kanazawa, and Matthew Tancik. Lerp: Language embedded radiance fields. In *ICCV*, 2023. 2, 5, 6

[16] Alexander Kirillov, Eric Mintun, Nikhila Ravi, Hanzi Mao, Chloe Rolland, Laura Gustafson, Tete Xiao, Spencer Whitehead, Alexander C. Berg, Wan-Yen Lo, Piotr Dollár, and Ross Girshick. Segment anything. *arXiv preprint arXiv:2304.02643*, 2023. 3

[17] Dmytro Kotovenko, Olga Grebenkova, and Björn Ommer. Edgs: Eliminating densification for efficient convergence of 3dgs. *arXiv preprint arXiv:2504.13204*, 2025. 2

[18] Abhijit Kundu, Kyle Genova, Xiaoqi Yin, Alireza Fathi, Caroline Pantofaru, Leonidas Guibas, Andrea Tagliasacchi, Frank Dellaert, and Thomas Funkhouser. Panoptic neural fields: A semantic object-aware neural scene representation. *arXiv preprint arXiv:2205.04334*, 2022. 2

[19] Vincent Leroy, Yohann Cabon, and Jerome Revaud. Grounding image matching in 3d with mast3r. In *ECCV*, 2024. 2

[20] Haijie Li, Yanmin Wu, Jiarui Meng, Qiankun Gao, Zhiyao Zhang, Ronggang Wang, and Jian Zhang. Instancegaussian: Appearance-semantic joint gaussian representation for 3d instance-level perception. In *CVPR*, 2025. 2

[21] Ben Mildenhall, Pratul P. Srinivasan, Matthew Tancik, Jonathan T. Barron, Ravi Ramamoorthi, and Ren Ng. Nerf: Representing scenes as neural radiance fields for view synthesis. In *ECCV*, 2020. 2

[22] Thomas Müller, Alex Evans, Christoph Schied, and Alexander Keller. Instant neural graphics primitives with a multiresolution hash encoding. In *ACM Trans. Graph.*, 2022. 2

[23] Phuc D. A. Nguyen, Tuan Duc Ngo, Evangelos Kalogerakis, Chuang Gan, Anh Tran, Cuong Pham, and Khoi Nguyen. Open3dis: Open-vocabulary 3d instance segmentation with 2d mask guidance. In *CVPR*, 2024. 2

[24] Maxime Oquab, Timothée Darcet, Théo Moutakanni, Huy Vo, Marc Szafraniec, Vasil Khalidov, Pierre Fernandez, Daniel Haziza, Francisco Massa, Alaaeldin El-Nouby, Mahmoud Assran, Nicolas Ballas, Wojciech Galuba, Russell Howes, Po-Yao Huang, Shang-Wen Li, Ishan Misra, Michael Rabbat, Vasu Sharma, Gabriel Synnaeve, Hu Xu, Hervé Jegou, Julien Mairal, Patrick Labatut, Armand Joulin, and Piotr Bojanowski. Dinov2: Learning robust visual features without supervision. *arXiv preprint arXiv:2304.07193*, 2024. 3

[25] Songyou Peng, Kyle Genova, Chiyu "Max" Jiang, Andrea Tagliasacchi, Marc Pollefeys, and Thomas Funkhouser. Openscene: 3d scene understanding with open vocabularies. In *CVPR*, 2023. 2

[26] Jens Piekenbrinck, Christian Schmidt, Alexander Hermans, Narunas Vaskevicius, Timm Linder, and Bastian Leibe. Opensplat3d: Open-vocabulary 3d instance segmentation using gaussian splatting. *arXiv preprint arXiv:2506.07697*, 2025. 2

[27] Minghan Qin, Wanhua Li, Jiawei Zhou, Haoqian Wang, and Hanspeter Pfister. Langsplat: 3d language gaussian splatting. In *CVPR*, 2024. 2

[28] Yansong Qu, Shaohui Dai, Xinyang Li, Jianghang Lin, Lijuan Cao, Shengchuan Zhang, and Rongrong Ji. Goi: Find 3d gaussians of interest with an optimizable open-

vocabulary semantic-space hyperplane. *arXiv preprint arXiv:2405.17596*, 2024. [2](#)

[29] Alec Radford, Jong Wook Kim, Chris Hallacy, Aditya Ramesh, Gabriel Goh, Sandhini Agarwal, Girish Sastry, Amanda Askell, Pamela Mishkin, Jack Clark, Gretchen Krueger, and Ilya Sutskever. Learning transferable visual models from natural language supervision. *arXiv preprint arXiv:2103.00020*, 2021. [2, 3](#)

[30] Adam Rashid, Satvik Sharma, Chung Min Kim, Justin Kerr, Lawrence Yunliang Chen, Angjoo Kanazawa, and Ken Goldberg. Language embedded radiance fields for zero-shot task-oriented grasping. In *CoRL*, 2023. [2](#)

[31] Paul-Edouard Sarlin, Daniel DeTone, Tomasz Malisiewicz, and Andrew Rabinovich. Superglue: Learning feature matching with graph neural networks. In *CVPR*, 2020. [2](#)

[32] Hongyu Shen, Junfeng Ni, Yixin Chen, Weishuo Li, Mingtao Pei, and Siyuan Huang. Trace3d: Consistent segmentation lifting via gaussian instance tracing. In *ICCV*, 2025. [2](#)

[33] William Shen, Ge Yang, Alan Yu, Jansen Wong, Leslie Pack Kaelbling, and Phillip Isola. Distilled feature fields enable few-shot language-guided manipulation. *arXiv preprint arXiv:2308.07931*, 2023. [2](#)

[34] Jin-Chuan Shi, Miao Wang, Hao-Bin Duan, and Shao-Hua Guan. Language embedded 3d gaussians for open-vocabulary scene understanding. *arXiv preprint arXiv:2311.18482*, 2023. [2](#)

[35] Wei Sun, Yanzhao Zhou, Jianbin Jiao, and Yuan Li. Cags: Open-vocabulary 3d scene understanding with context-aware gaussian splatting. *arXiv preprint arXiv:2504.11893*, 2025. [2](#)

[36] Stanislaw Szymanowicz, Christian Rupprecht, and Andrea Vedaldi. Splatter image: Ultra-fast single-view 3d reconstruction. In *CVPR*, 2024. [2](#)

[37] Ayça Takmaz, Elisabetta Fedele, Robert W. Sumner, Marc Pollefeys, Federico Tombari, and Francis Engelmann. Open-mask3d: Open-vocabulary 3d instance segmentation. In *NeurIPS*, 2023. [2](#)

[38] Shuzhe Wang, Vincent Leroy, Yohann Cabon, Boris Chidlovskii, and Jerome Reaud. Dust3r: Geometric 3d vision made easy. In *CVPR*, 2024. [2](#)

[39] Yanmin Wu, Jiarui Meng, Haijie Li, Chenming Wu, Yahao Shi, Xinhua Cheng, Chen Zhao, Haocheng Feng, Errui Ding, Jingdong Wang, and Jian Zhang. Opengaussian: Towards point-level 3d gaussian-based open vocabulary understanding. In *NeurIPS*, 2024. [2, 7](#)

[40] Kashu Yamazaki, Taisei Hanyu, Khoa Vo, Thang Pham, Minh Tran, Gianfranco Doretto, Anh Nguyen, and Ngan Le. Open-fusion: Real-time open-vocabulary 3d mapping and queryable scene representation. *arXiv preprint arXiv:2310.03923*, 2023. [2](#)

[41] Chi Yan, Delin Qu, Dan Xu, Bin Zhao, Zhigang Wang, Dong Wang, and Xuelong Li. Gs-slam: Dense visual slam with 3d gaussian splatting. In *CVPR*, 2024. [2](#)

[42] Mingqiao Ye, Martin Danelljan, Fisher Yu, and Lei Ke. Gaussian grouping: Segment and edit anything in 3d scenes. In *ECCV*, 2024. [2](#)

[43] Hongjia Zhai, Xiyu Zhang, Boming Zhao, Hai Li, Yijia He, Zhaopeng Cui, Hujun Bao, and Guofeng Zhang. Splatloc: 3d gaussian splatting-based visual localization for augmented reality. *arXiv preprint arXiv:2409.14067*, 2024. [2](#)

[44] Shijie Zhou, Haoran Chang, Sicheng Jiang, Zhiwen Fan, Zehao Zhu, Dejia Xu, Pradyumna Chari, Suya You, Zhangyang Wang, and Achuta Kadambi. Feature 3dgs: Supercharging 3d gaussian splatting to enable distilled feature fields. In *CVPR*, 2024. [2](#)

ProFuse: Efficient Cross-View Context Fusion for Open-Vocabulary 3D Gaussian Splatting

Supplementary Material

A. Reproducibility and Code Release

The implementation of ProFuse will be released at <https://github.com/chiou1203/ProFuse>. This repository will include the training code for the dense correspondence guided Gaussian initialization, cross-view mask clustering, and feature registration stages.

B. Discussion

B.1. Limitation

Although cross-view mask clustering helps associate masks that likely refer to the same context, our method still remains bounded by SAM and CLIP. Mask embeddings still reflect the underlying segmentation quality. Moreover, even with accurately segmented masks, CLIP embedding errors directly affect 3D scene understanding, particularly for similar objects and uncommon text prompts.

Though pre-registration is correspondence driven, even with warps, mismatches can persist when masks are imperfect. For example, under an IoU threshold of 0.5, a mask that is 80% a large object and 20% a small object may be grouped with other masks of the large object; the pooled global feature then inherits contamination from the small object. This relates to over-coarse grouping in which masks group that are not clean and highly accurate washed out fine details and an inaccurate global feature can pollute all its mask members.

B.2. Societal Impact

The method lowers the barrier to open vocabulary understanding in 3D scenes. It attaches language descriptors to Gaussians through correspondence driven pre-registration and feature registration without a render supervised loop. The result is shorter iteration time and a lighter compute footprint. These gains translate into practical uses. Education and cultural heritage benefit from interactive exploration of reconstructed spaces where a user can ask for an object and see it in context. AR and VR authors gain a searchable index over large captures that enables precise selection and editing without project specific training. Robotics and digital twins obtain faster scene lookup for inventory, maintenance, and task setup in indoor environments. Assistive scenarios become more responsive since a user can request a target item and receive immediate guidance in a captured room.

Responsible deployment remains straightforward. Capture and indexing should follow clear consent. Storage and sharing should use established governance in each setting. With these norms in place, ProFuse helps democratize semantic interaction with 3D content and broadens access to practical tools for learning, creation, and operation.

C. Preliminaries

C.1. 3D Gaussian Splatting

3D Gaussian Splatting represents a scene with a set of anisotropic Gaussians. Each primitive has a mean in world space and a covariance that is factorized into a rotation and a diagonal scale. This factorization guarantees a valid positive semi-definite matrix and is convenient for optimization.

Rendering proceeds by projecting each 3D covariance to image space through a first-order camera Jacobian, which yields a 2×2 covariance for splatting on the raster plane. The pixel color is then obtained by front-to-back alpha compositing. The formulation matches volumetric rendering and can be written as a sum of per-splat contributions, where the contribution of the i -th splat equals its transmittance times its effective opacity times its color. Transmittance accumulates along the ray as the product of one minus the previous opacities.

The original system uses a differentiable tile-based rasterizer. Gaussians are culled against the frustum and tiles, sorted by depth, and blended per tile to maximize parallelism while maintaining the same alpha-compositing model.

C.2. Product Quantization (PQ)

ProFuse follows Dr.Splat who utilize Product Quantization to store and search language features efficiently without per-scene codebook training. PQ partitions a D -dimensional vector into L sub-vectors, learns a codebook per subspace, and represents each sub-vector by the index of its nearest centroid. This reduces memory and turns distance or similarity computation into table lookups across subspaces.

After training centroids, a lookup table stores all pairwise distances among centroids in each subspace. The distance between two PQ-encoded vectors becomes a sum

of L table entries, one per subspace. Cosine similarity can be computed in the same way using inner-product tables after normalizing subvectors. This design shifts the cost from high-dimensional arithmetic to indexed retrieval while preserving correlation with true distances within known quantization bounds.

Significant search-time gains over direct cosine similarity on CLIP features can be observed when varying the sub-vector size. These measurements demonstrate that LUT-based PQ search scales well for large 3D Gaussian sets and supports interactive text-to-3D queries.

D. Implementation Details

D.1. Correspondence Driven Gaussians

Unlike standard 3DGS, we initialize the scene from dense cross-view correspondences and then perform a pruning-only optimization without densification. A trainer calls a correspondence-based initializer and proceeds with a photometric objective under a fixed training schedule.

We first sample a compact set of reference views by K-means clustering in pose space to cover the trajectory with minimal redundancy. For each reference we attach a small pose-nearest neighbor set, selected by distance in the same pose space. We sample a set of reference views and attach a small pose-nearest set of neighbors to each reference. In our runs, we use 180 reference views and 3 neighbors per reference for maximum efficiency. The initializer computes a dense warp field and certainties of each warp, aggregates the most confident warp per pixel, and triangulates 15,000 correspondences per reference to seed Gaussians. The seed carries position, color, and scale from the paired views, followed by standard splat optimization. We enable pruning while disabling densification during training, removing poor splats without ever growing new ones. Opacity resets are effectively off through a very large reset interval. We use a batch size of 64 and run 30,000 iterations per scene. This procedure typically yields around 2×10^6 initialized Gaussians and roughly 5×10^5 to 10^6 active Gaussians after pruning.

D.2. The ProFuse Framework

ProFuse attaches language descriptors to a Gaussian scene that is initialized from dense correspondences and refined with pruning only. The representation follows standard 3D splatting for geometry and visibility. The semantic path operates on masks and text features and produces a per-Gaussian descriptor that supports open-vocabulary queries without a render-supervised loop.

Masks come from the object level of SAM. Each mask is encoded by CLIP ViT-H/14 with a 512-dimensional embedding. Per-view features are fused to Gaussians using the Top-K ray contributions from the renderer so the same

weights that produce color also produce language features. The fusion creates a single descriptor per Gaussian that is shared across views and does not depend on any prompt at training time.

Descriptors are stored with Product Quantization. We use a global codebook that is shared across all scenes and keep the PQ codes as the only per-Gaussian semantic payload during training and inference. The system reconstructs codes to unit-norm vectors for cosine scoring when answering a text query. This design reduces memory and enables fast similarity evaluation while keeping the scoring rule identical to the one used for visualization and selection.

D.3. Compare Model Settings

LangSplat. LangSplat learns a 3D language field on 3D Gaussians and replaces NeRF rendering with tile-based splatting for language features. It builds a scene-wise language autoencoder and trains language features in a scene-specific latent space rather than directly on CLIP space, which reduces memory. Supervision comes from SAM to form hierarchical semantics so that subpart, part, and whole concepts are separable. The paper reports large speed gains over LERF at high resolution, which is consistent with the splatting design and the latent-space training.

LEGaussians. LEGaussians discretizes language features with a learnable codebook and stores indices rather than full float descriptors. Quantization selects the nearest basis in a discrete feature space using a CLIP term and a controllable DINO term; optimization aligns dense image features to their quantized counterparts. During training the method renders compact semantic vectors from Gaussians and decodes them with a small MLP under a cross-entropy objective. It further adds adaptive spatial smoothing driven by a learned per-Gaussian uncertainty so that semantics vary smoothly where features are unstable. These design choices reduce storage and regularize multi-view inconsistency.

OpenGaussian. OpenGaussian augments each Gaussian with a low-dimensional instance feature and learns it by rendering feature maps with alpha blending. Supervision uses SAM boolean masks without cross-view correlation. The loss encourages intra-mask smoothness and inter-mask separation so that features within an object cluster together while different objects separate in feature space. To discretize for efficient retrieval, a two-level codebook is constructed in a coarse-to-fine manner. The coarse stage clusters by concatenating position with features; the fine stage clusters by features only, which preserves geometry and improves scalability in larger scenes. The paper also proposes an instance-level association that links 2D CLIP to 3D points without additional training.

Dr. Splat. Dr. Splat performs direct feature registration on pre-trained 3DGS scenes. Per-pixel CLIP embeddings are aggregated onto the dominant top- k Gaussians along each camera ray with weights equal to transmittance times effective opacity from the volume rendering equation. The aggregated embeddings are product-quantized and stored as PQ indices, enabling compact storage and fast 3D search without per-scene feature distillation. The paper contrasts this registration-based pipeline with rendering-supervised methods and reports substantially shorter end-to-end preparation and query times.

D.4. Training Details

Dense Correspondence. The settings for dense correspondence are shown in Table 1. We select 180 reference views by K-means in pose space and attach 3 pose-nearest neighbors to each reference by k-NN. We use RoMa as the pretrained network for dense matches. We cap the sampling at 15,000 matches per reference. Certainty is aggregated by a per-pixel maximum across neighbors.

Gaussian Initialization. The Gaussian initialization and optimization settings are summarized in Table 2. Each correspondence track is triangulated with calibrated cameras, and we keep only tracks whose mean reprojection error is below 0.01 in normalized image coordinates. For every surviving 3D point we create a Gaussian with spherical covariance, where the initial scale parameters are set to 0.001 in scene units.

Gaussian Optimization. The initialized scene is then optimized with the 3DGS training loop for 30,000 iterations with batch size 64. The position learning rate starts at 1.6×10^{-4} and decays to 1.6×10^{-6} over 30,000 steps with a delay multiplier of 0.01. The feature learning rate is 0.0025, the opacity learning rate is 0.025, the scaling learning rate is 0.005, and the rotation learning rate is 0.001. We keep the dense ray sampling ratio at 1 % of pixels per iteration (percent_dense = 0.01) and weight the DSSIM term by 0.2. Densification itself is disabled by setting no_densify to True. The opacity reset interval is extended to 1,000,000 iterations so that no opacity reset occurs during optimization.

Cross-View Mask Clustering. After dense feature matching, we cluster masks that likely depict the same scene region across views. For each reference image, we use SAM mask level 1 as the object-level partition. The reference segmentation is resized to the RoMa canvas resolution, and each neighbor segmentation is projected into this canvas using the warp. We prune projected labels with the Gaussian visibility mask, using a transmittance threshold of 0.05. The warped IoU threshold for cluster edges are set to 0.2 and bounding box IoU 0.08. Very small masks that cover less than 0.5% of the canvas use a stricter IoU requirement of 0.30 in order to avoid spurious links

caused by noise. Connected components in this graph define the cross-view clusters, and for each reference image we store the cluster assignments and corresponding SAM label ids in a NPZ file that is reused by the registration stage.

Table 1: Dense correspondence setting.

Config	Value
Dense Matching Network	RoMa
Total References	180
Neighbors per Reference	3
Max Matches per Reference	15,000

Table 2: Gaussian pre-training setting.

Config	Value
Triangulation Reprojection	
Tolerance	0.01
Initial Scale	0.001
Training Iterations	30,000
Batch Size	64
Optimizer	Adam
Base Position Learning Rate	1.6×10^{-4}
Delay Multiplier	0.01
Feature Learning Rate	0.0025
Opacity Learning Rate	0.0025
Scaling Learning Rate	0.005
Rotation Learning Rate	0.001
Percent Dense Pixels	0.01
DSSIM weight	0.2
Densification	Disabled

Table 3: Cross-view mask clustering setting.

Config	Value
SAM Mask Level	1 (Object)
Visibility Threshold	0.05
Warped IoU	0.2
Bounding Box IoU	0.08
Small Mask Fraction	0.005
Small Mask IoU	0.3
Edge Requirement	Mutual Best Neighbor

Table 4: Feature registration setting.

Config	Value
Feature Level	1
Top-K	10
PQ Index	128-D
Pixel Stride	1
SpMM Cluster Block	0
Eps Contribution	0

Feature Registration. Settings for registration are summarized in Table 4. During registration, we freeze the Gaussian scene and run a single registration pass that attaches a 512-dimensional language descriptor with feature level 1 to every Gaussian. Proposal-level feature registration is used whenever a valid NPZ file is available and the code falls back to per-mask accumulation only when a view has no mapped cluster metadata.

For each camera, we render the top-10 Gaussian ids and their contributions per pixel from the pretrained scene. To control sampling density on clustered pixels, we introduce pixel stride. Valid pixels inside clustered masks are sub-sampled with a uniform stride in image space, keeping the option for heavier scenes if needed. After collecting top-10 contributions for these pixels, we build a sparse weight matrix between Gaussians and cluster ids. Before forming this matrix, we apply a small threshold on contributions through `eps_contrib`. Entries with contribution below this threshold are discarded, which removes numerically tiny pairs that only add memory cost but almost no semantic signal. We set default stride to 1 and `eps_contrib` to 0 in reported experiments.

The accumulation is implemented as a sparse matrix-dense matrix multiplication over Gaussians and global features. An optional parameter `spmm_cluster_block` allows the cluster axis to be processed in blocks when GPU memory is tight. Each block builds a smaller sparse matrix for a subset of clusters and accumulates the result into the global Gaussian buffers. We set `spmm_cluster_block` = 0 in all our runs since our scenes fit comfortably within memory at this resolution.

Once the per-Gaussian float features are obtained, we normalize them and encode them with product quantization. We always enable PQ and load a pretrained FAISS index with code size 128. The final stored language descriptor of each Gaussian is a 128-byte PQ code.

D.5. Evaluation Details

Open-Vocabulary 3D Object Selection. We adopt the LERF object selection benchmark and use the same four scenes, prompts, and binary ground-truth masks as in Section 4.2. For each method we compute cosine similarity between every Gaussian language descriptor and the CLIP text embedding of the query. Gaussians are activated when the similarity exceeds a threshold τ . In practice, τ is chosen for each method by grid search, sweeping values in steps of 0.01 and fixing the best value across all scenes. The re-ranking stage follows the LERF relative-relevance formulation with the canonical word list {object, things, stuff, texture} and temperature $\tau_{\text{rerank}} = 3.0$. After selecting Gaussians, we aggregate their per-pixel contribution weights thresholding at a contribution level

$\gamma = 0.025$. We then compute mIoU and mAcc@0.25 on the same set as LERF and average the scores over all scenes.

Open-Vocabulary 3D Point Cloud Understanding.

For ScanNet dataset, we evaluate all methods on the 19-class, 15-class, and 10-class label sets with a strict point-level protocol. For each checkpoint we decode the 512-dimensional PQ language features back to float vectors using the original FAISS index. Codes that are all-255 or mapped to an invalid IVF list are treated as invalid, decoded features are L2-normalized, and invalid rows are kept as zeros. Class text features are loaded from an JSON, aligned to the class name list for each label set, and L2-

Table 5: Evaluation setting.

Config	Value
Contribution Threshold	0.025
Reranking Temperature	3
Gaussian Candidates	64
Gating Radius	3
SoftMax Temperature	1

normalized. We form cosine logits between all Gaussians and all class text features and transfer these logits to mesh vertices using the rotation- and scale-aware Mahalanobis kernel with opacity weighting. The kernel uses a shortlist of $k_{\text{shortlist}} = 64$ Gaussian candidates per point, a gating radius $\sigma_{\text{gate}} = 3.0$ in Mahalanobis distance, and a SoftMax temperature $\text{logit_temp} = 1.0$; these values are shared by the 19-class, 15-class, and 10-class evaluators. Points that fall outside the σ_{gate} fall back to the nearest valid Gaussian. We report point-mIoU and point-mAcc averaged over classes that are present in the ground truth and over the evaluation scenes listed in Section 4.3.

D.6. Computing Resource Configuration

The experiments of ProFuse were conducted on a single NVIDIA A100 80 GB GPU. All methods were evaluated with their best model on their best threshold to maintain consistency. ScanNet scenes are down sample to 170 ~ 210 images per scene, and each Gaussian scene was trained for 30k iterations with the same hyper-parameter setting during scene optimization. The experiments on registration-based methods were compared using the same PQ codebook with sub-vector size 128, and best threshold were picked method-wise to respect different model nature, ensuring a comprehensive and uniform assessment of performance across different architectures.

E. Additional Experiments

E.1. Gaussian Scene Experiments

We investigate how the choice of pretrained Gaussian scene affects both reconstruction quality and semantic association. Three variants are evaluated under the same ProFuse registration pipeline and object-selection protocol, as summarized in Tables 6–9. The first variant applies ProFuse on top of a standard SfM-based 3D Gaussian Splatting scene. Dense correspondence and cross-view mask clustering are still computed, but these tracks only influence the semantic side; the underlying geometry follows the original 3DGS training procedure. The second variant is the default ProFuse configuration used in the main paper. In this case the Gaussian scene is initialized from dense correspondence tracks without densification, followed by our 30k-step pruning-only optimization. The third variant enables densification on top of the correspondence-guided seeds.

Scene-level mIoU and mAcc@0.25 for the LERF object-selection task are reported in Tables 6 and 7. The correspondence-guided scene without densification consistently improves over the pure 3DGS scene in both metrics, and achieves the best mean semantic performance across the four scenes. Enabling densification yields mixed behavior. Some scenes remain competitive, while others suffer from a noticeable drop in mIoU and mAcc. We attribute this to the strong variation of the similarity-threshold curve across scenes. A single global activation threshold is applied within each variant, which is a reasonable choice for comparison but cannot simultaneously track the per-scene optimum once the density pattern of Gaussians changes significantly.

Table 8 reports PSNR of the rendered views from the three pretrained scenes. Here the correspondence-guided initialization with densification achieves the highest mean PSNR, while the non-densified ProFuse scene is slightly below. This indicates that densification still brings benefits for pure reconstruction, even when the initial seeds already introduce highly accurate geometry.

Table 9 further compares the optimization time across scenes. The correspondence-guided scene without densification shortens training to roughly 14 minutes on average. Enabling densification increases the mean time to about 22 minutes, almost doubling the cost on some scenes. Combining these trends, the default ProFuse configuration, which uses correspondence-guided seeds without densification, forms a practical compromise. It delivers the strongest semantic performance in the object-selection benchmark, preserves competitive reconstruction quality, and keeps the pretraining time significantly lower than the densified alternative.

Qualitative example of the scene reconstruction progress for correspondence-guided 3DGS is illustrated

in Figure 1. The left shows the reference image. The second column renders the raw seeds produced directly from dense correspondence before any optimization, already capturing the layout of major objects. The third column shows the scene after 7k optimization steps of pruning, where geometry and appearance become noticeably sharper. The right column visualize the result after 30k iterations, which mainly refines shading and small details. This qualitative behavior is consistent with the quantitative results and illustrates that correspondence-guided initialization provides a strong geometric prior even without densification

Table 6: Ablation study on scene mIoU for different pretrain Gaussian scenes.

Gaussian Scene	Scene mIoU				
	Waldo kitchen	Figurines	Ramen	Teatime	Mean
3DGS	24.45	55.27	24.70	62.57	41.75
Corr-init	36.91	56.13	28.16	62.78	46.00
Corr-init + Densify	14.29	41.31	28.16	60.62	36.10

Table 7: Ablation study on scene mAcc for different pretrain Gaussian scenes.

Gaussian Scene	Scene mAcc@0.25				
	Waldo kitchen	Figurines	Ramen	Teatime	Mean
3DGS	36.36	83.93	40.85	79.66	59.85
Corr-init	68.18	85.71	39.44	79.66	68.25
Corr-init + Densify	22.72	67.86	39.44	79.66	52.42

Table 8: Ablation study on scene PSNR for different pretrain Gaussian scenes.

Gaussian Scene	Scene PSNR				
	Waldo kitchen	Figurines	Ramen	Teatime	Mean
3DGS	32.89	24.95	28.73	31.39	29.49
Corr-init	32.18	24.61	28.84	31.52	29.29
Corr-init + Densify	34.65	26.34	30.02	32.73	30.94

Table 9: Optimization time analysis on enabling densification for Gaussian optimization of ProFuse pretrained scene.

Densification	Optimization Time				
	Waldo kitchen	Figurines	Ramen	Teatime	Mean
W/O Densify	~13m	~12m	~14m	~15m	~14m
Densify	~27m	~23m	~16m	~24m	~22m

Reference Initialization 7k Iterations 30k Iterations

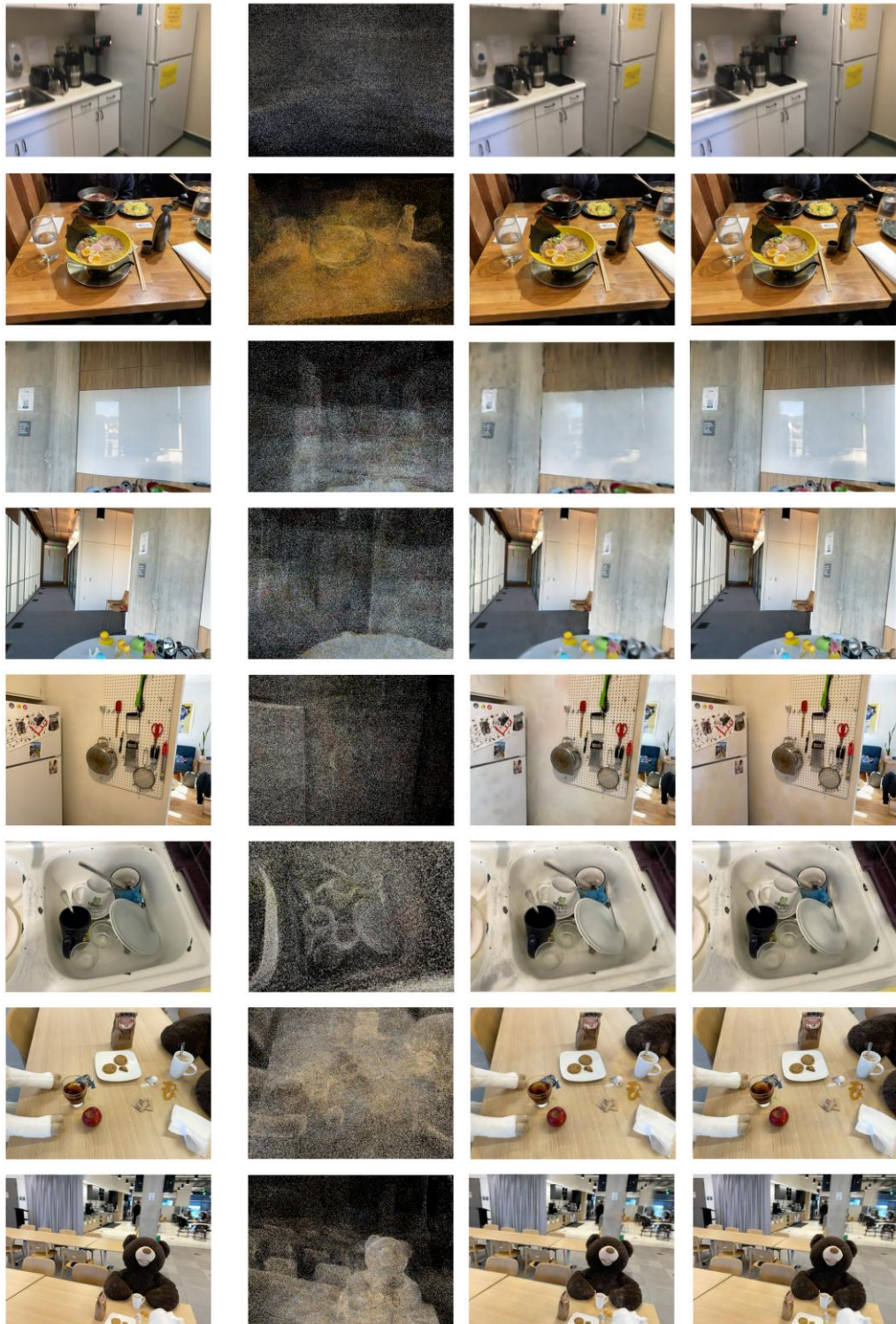


Figure 1. Correspondence-based scene reconstruction of ProFuse.

E.2. Neighbor per Reference

We study how the number of neighbors per reference view influences both semantic understanding and the cost of dense correspondence. The experiment varies the neighbor count in pre-registration stage, using values 0, 3, 5, 7, and 9 while keeping all other components fixed. Setting the neighbor count to 0 disables cross-view mask clustering and therefore removes 3D Context Proposals, leaving solely correspondence-guided Gaussian initialization. The remaining settings preserve both the correspondence-based initialization and the context proposal pipeline, with increasingly large neighborhood graphs.

Tables 11 and 12 report scene-level mIoU and mAcc@0.25 on the LERF object selection task. Comparing 0 and 3 neighbors shows that introducing even a small neighborhood already improves mIoU noticeably, which confirms that the gain of ProFuse over the registration baseline is not explained only by a different pretrained Gaussian scene. The additional global feature injected by 3D context proposals genuinely strengthens semantic association. As the neighbor count grows beyond 3, several scenes exhibit further improvements in mIoU, while the Figurines scene becomes slightly less stable, suggesting that very large neighborhoods may introduce noisy cross-view links for cluttered layouts. Overall increase in mIoU indicates that richer cross-view evidence can still benefit the registration stage.

The mAcc@0.25 curves show a more nuanced behavior. Waldo kitchen is a representative example. Its mIoU increases significantly when the neighbor count exceeds 3, yet its mAcc decreases slightly. This apparent contradiction is explained by the threshold-selection procedure. For each variant we fix a single activation threshold shared across scenes. The mIoU of Waldo kitchen as a function of the threshold forms a curve whose peak shifts toward lower thresholds when the neighborhood grows. The global threshold chosen for the ablation lies farther from this new peak, so the reported mAcc does not fully reflect the best possible accuracy of the scene. In practice Waldo kitchen can reach mIoU above 46 and mAcc above 68 under a threshold tuned specifically for that configuration, which is consistent with the improved curve.

Table 13 summarizes the initialization time of the dense correspondence stage. The cost grows steadily with the neighbor count, since every additional neighbor requires extra RoMa evaluation and mask projection. Different scenes exhibit slightly different sensitivity, but the trend is consistent. When we compare the average semantic gains against the additional time, three neighbors per reference offers a favorable trade-off, keeping the pre-registration stage within a practical budget.

Table 10: Ablation study on scene mIoU for different neighbor per reference.

Neighbors	Scene mIoU				
	Waldo kitchen	Figurines	Ramen	Teatime	Mean
0	33.80	48.28	25.09	57.57	41.19
3	36.91	56.13	28.16	62.78	46.00
5	40.89	50.06	29.29	64.99	46.31
7	43.08	49.31	28.99	65.10	46.62
9	43.51	49.15	29.10	65.04	46.7

Table 11: Ablation study on scene mAcc for different neighbor per reference.

Neighbors	Scene mAcc@0.25				
	Waldo kitchen	Figurines	Ramen	Teatime	Mean
0	63.64	82.14	38.03	77.97	64.45
3	68.18	85.71	39.44	79.66	68.25
5	50.00	83.93	40.85	79.66	63.61
7	54.54	82.14	40.85	79.66	64.30
9	54.54	82.14	40.85	79.66	64.30

Table 12: Ablation Study on Dense correspondence initialization time with different neighbor per reference

Neighbors	Scene Init Time				
	Waldo kitchen	Figurines	Ramen	Teatime	Mean
3	2m 29s	2m 37s	1m 40s	1m 47s	2m 08s
5	4m 1s	3m 43s	3m 18s	3m 51s	3m 44s
7	3m 58s	6m 21s	3m 47s	5m 35s	4m 25s
9	7m 11s	8m 4s	4m 52s	6m 53s	6m 23s

E.3. Additional Ablations

More Details on Top-K Choice. Top-K ablations for ScanNet point-cloud understanding with 10 labeled classes were discussed in Section 4.5. The same behavior also applied to 19 and 15 classes label sets. Under the same evaluation protocol, ProFuse reaches its best or near-best mIoU and mAcc within top-10 Gaussians, while the Dr. Splat baseline continues to improve when K is increased and usually needs K=40 to approach its own peak. This contrast indicates that our proposal-based registration concentrates the useful semantic mass on a much smaller subset of Gaussians along each ray and is therefore far more efficient.

We seek to find direct evidence for this concentration and whether the outcome is healthy by analyzing the contribution mass of each scene. For each ScanNet scene, we record the per-view “top-10 share” during registration. For each view, a vector is built where each entry is the total contribution weight assigned to one context proposal in that view. We then derive top 10 share as

$$\frac{\text{mass of 10 largest proposals}}{\text{total mass of all proposals}}.$$

The resulting mass for each view ranges between 0.87 and 0.99, which means that the 10 most active proposals already account for the majority of the total proposal mass in a typical view. At the scene level, we also compare the fraction of total Gaussian mass that lies in the most heavily used 0.1% and 1% of Gaussians. The top 1% of Gaussians carries between 41 ~ 68% of the accumulated contribution mass, and the top 0.1% still carry 14 ~ 42%. These statistics show that both clusters and Gaussians exhibit a highly skewed distribution under our registration scheme, which explains why ProFuse saturates at $K=10$ on all three ScanNet label sets, whereas Dr. Splat requires much larger K to reach comparable point-cloud performance.

Warped IoU. We ablate the warped intersection-over-union threshold τ_{iou} that decides whether a dense-warped mask pair contributes an edge to the cluster graph. The threshold is varied in $\{0.1, 0.2, 0.3, 0.4, 0.5\}$ and for each value we recompute 3D context proposals and repeat the object-selection and point cloud evaluation. The resulting scene-level mIoU curves are not monotonic, and the behavior differs across scenes, which suggests that the effective operating point is shaped by a combination of warped IoU and the mutual best-neighbor rule. Once mutual best neighbors are enforced, many noisy correspondences are removed before the IoU gate is applied, resulting in τ_{iou} controls mainly a secondary pruning stage. In this regime $\tau_{iou} = 0.2$ provides a stable choice across scenes. It retains enough cross-view links to form reliable context proposals while still discarding clearly inconsistent warps, and we adopt this threshold as default setting for all main experiments.

Inferencing Efficiency. Removing densification and relying on correspondence-guided initialization leads to a much more compact Gaussian scene. Table 13 summarized the comparison of average inferencing time and total Gaussians per scene. On ScanNet, Dr. Splat keeps 2.7 times more Gaussians than our method while operating on the same data. Despite this reduction, the semantic and geometric metrics reported in the main paper remain competitive or improved, which indicates that the correspondence seeds and pruning schedule preserve the informative splats.

We also measure the cost of point-cloud inference on ScanNet. Under the same evaluation pipeline, Dr. Splat requires on average about 99 seconds per scene, whereas ProFuse completes the same retrieval in about 59 seconds. The method therefore achieves faster inference together with a substantially smaller Gaussian set, which matches the reduction in Gaussian count and confirms that the correspondence-initialized, non-densified scenes are advantageous both for efficiency and for downstream open-vocabulary understanding.

Table 13: Ablation study on inference efficiency.

Method	Inference Time/ Total Gaussians
Dr. Splat	99s / 1.27M
ProFuse	59s / 470K

E.4. More Qualitative Results

We provide additional qualitative results of ProFuse in this section. Figures 2 and 3 visualize cosine similarity activations for several text queries on LERF scenes. The results illustrate that global features sharpen the response on the queried object, suppress background clutter, and maintain consistent activation within the object extent. Figure 4 presents PCA projections of the per-Gaussian language features on ScanNet and LERF scenes. For each view we display the input image together with the projected features of Dr. Splat and ProFuse. The ProFuse features form more coherent regions that align much better with objects and surfaces and they remain stable across different viewpoints, which supports the improvements observed in the quantitative evaluations. Figure 5 illustrate feature visualization on more ScanNet scenes, demonstrating the strength of ProFuse in context understanding.

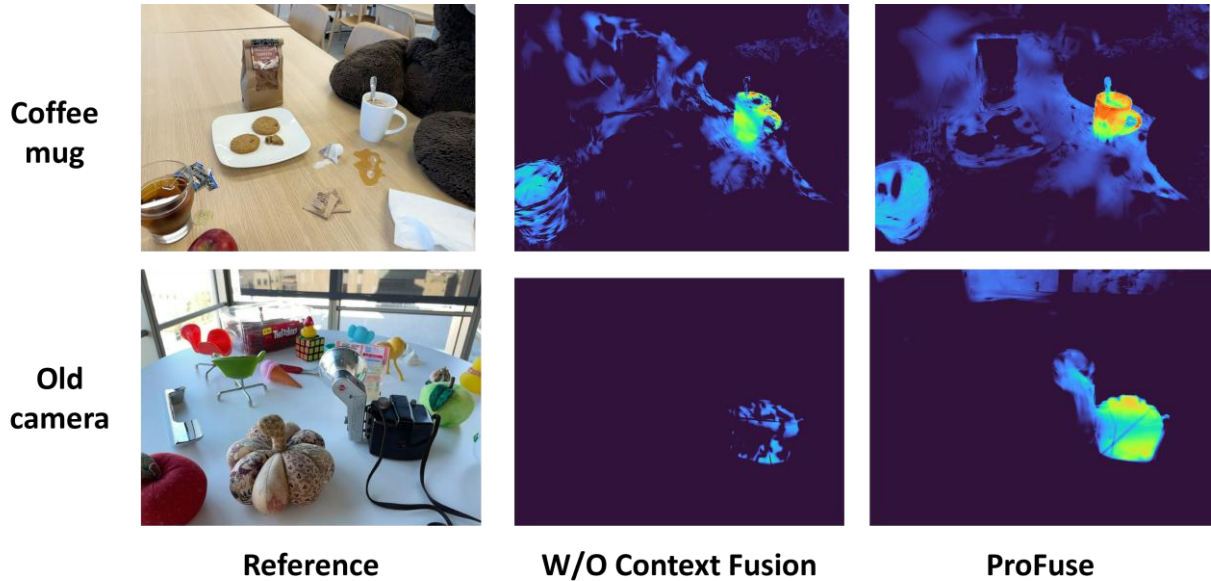


Figure 2. Qualitative results of cosine similarity activation on given queries “coffee mug” and “old camera”.

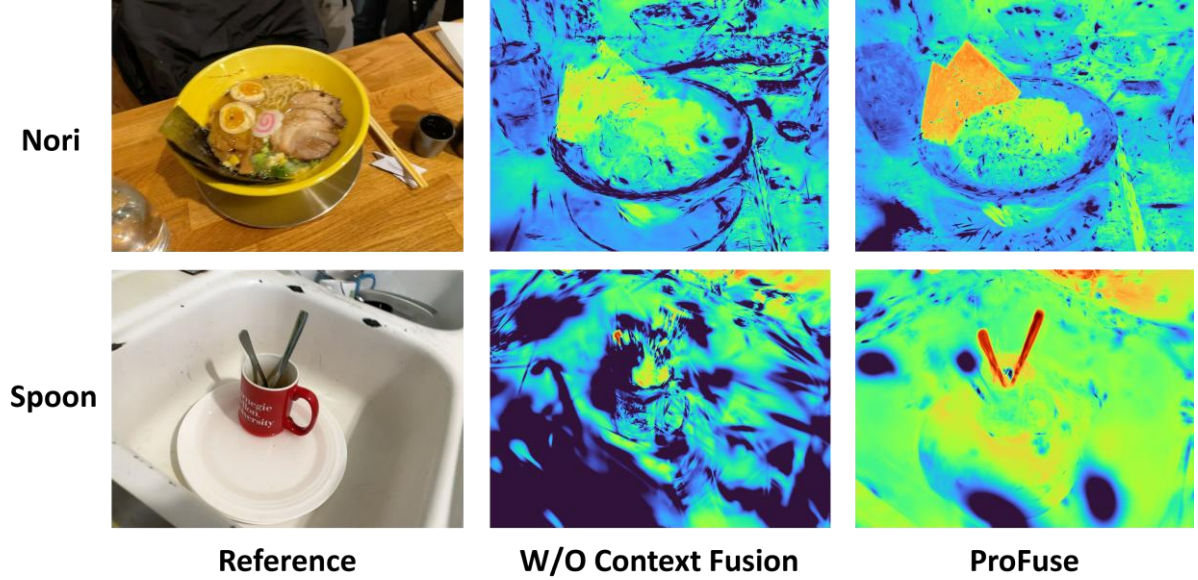


Figure 3. Qualitative results of cosine similarity activation on given queries “nori” and “spoon”. With global features, ProFuse carries context-level interpretation and injects consistency in 3D scene understanding.

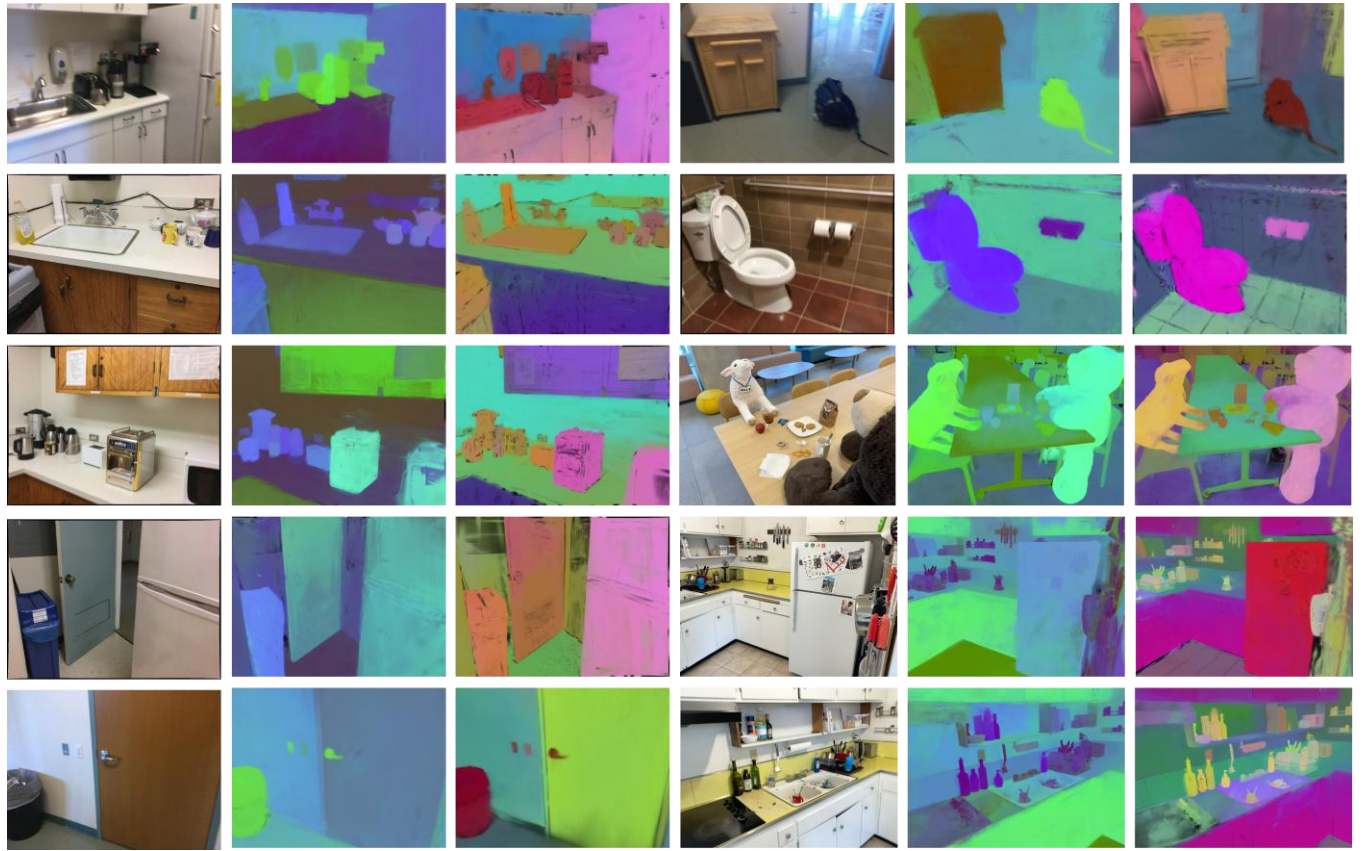


Figure 4. Qualitative results of PCA visualization on ScanNet and LERF scenes. For each view, we provide the reference image (left), and render PCA of Dr. Splat (middle), and ProFuse (right) for comparison.

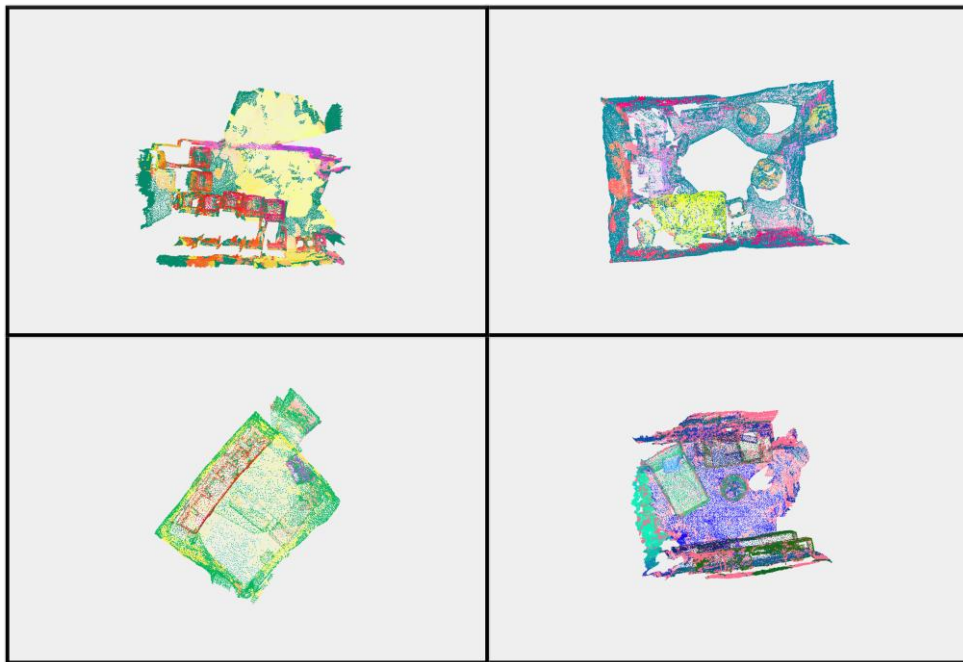


Figure 5. Additional rendering of feature visualization on ScanNet scenes.